Scanning Electrochemical Cell Microscopy (SECCM) Chronopotentiometry: Development and Applications in Electroanalysis and Electrocatalysis

Enrico Daviddi, Katerina L. Gonos, Alex W. Colburn, Cameron L. Bentley and Patrick R. Unwin**

Department of Chemistry, University of Warwick, Coventry CV4 7AL, U.K.

Scanning electrochemical cell microscopy (SECCM) has been applied for nanoscale (electro)activity mapping in a range of electrochemical systems, but so far has almost exclusively been performed in controlled-potential (amperometric/voltammetric) modes. Herein, we consider the use of SECCM operated in a controlled-current (galvanostatic or chronopotentiometric) mode, to synchronously obtain spatially-resolved electrode potential (*i.e.*, electrochemical activity) and topographical "maps". This technique is firstly applied, as proof of concept, to study the electrochemically reversible $[Ru(NH_3)_6]^{3+/2+}$ electron transfer process at a glassy carbon electrode surface, where the experimental data are in good agreement with well-established chronopotentiometric theory under quasi-radial diffusion conditions. The $[Ru(NH_3)_6]^{3+/2+}$ process has also been imaged at "aged" highly ordered pyrolytic graphite (HOPG), where apparently enhanced electrochemical activity is measured at the edge plane relative to the basal plane surface, consistent with potentiostatic measurements. Finally, chronopotentiometric SECCM has been employed to benchmark a promising electrocatalytic system, the hydrogen evolution reaction (HER) at molybdenum disulfide (MoS_2), where higher electrocatalytic activity (*i.e.*, lower overpotential at a current density of 2 mA cm^{-2}) is observed at the edge plane compared to the basal plane surface. These results are in excellent agreement with previous controlled-potential SECCM studies, confirming the viability of the technique and thereby opening up new possibilities for the use of chronopotentiometric methods for quantitative electroanalysis at the nanoscale, with promising applications in energy storage (battery) studies, electrocatalyst benchmarking and corrosion research.

Introduction

Scanning electrochemical cell microscopy (SECCM),[1] and earlier related scanning meniscus electrochemical cell techniques,[2] have proven to be very powerful for elucidating structure-activity in a wide range of electrochemically active (nano)materials,[3,4] including sp^2 carbon (*e.g.*, nanotubes, graphite and graphene),[5-7] (electro)catalytic materials (*e.g.*, polycrystalline metals,[8,9] nanoparticles,[10-12] molybdenum disulfide[11,13] and iron nickel sulfides[14]), materials for energy storage[15] and composite materials of interest in corrosion science.[16] SECCM employs an electrolyte filled micropipet or nanopipet, also containing quasi-reference counter electrode(s) (QRCEs), as the probe. The pipet is used to make meniscus contact with the surface of interest, creating a confined electrochemical cell via a "droplet" cell at the tip of the probe. Localized electrochemical measurements are made at a series of points across the surface to build up a spatially-resolved map (or movie) of electrochemical reactivity and synchronous topography at the micro/nanoscale.[4,17,18]

SECCM was originally mainly deployed in a constant-distance scanning mode, where the probe was translated across the surface of interest (conventional raster-scan and later high-speed spiral scan patterns employed[10]) at a constant rate to obtain spatially-resolved (electro)chemical information.[4,17] In this configuration, a dual-channel probe was used, and an ionic current (i_{ionic}), induced by applying a bias between the two-channels, served as an independent feedback signal to position the probe (*i.e.*, maintain a constant-distance) relative to the surface of interest. A "hopping-mode" protocol was later adopted,[13,19,20] where the dual-channel probe (i_{ionic} again serving as the feedback signal) was approached to the substrate surface at a series of predefined locations in a grid and, upon each landing, an independent voltammetric measurement (*e.g.*, linear-sweep voltammetry, cyclic voltammetry and chronoamperometry) was made, building-up a voltammetric 'map' of the substrate. It should be noted that while the use of a dual-channel probe (*i.e.*, i_{ionic} feedback) in "hopping-mode"

allows non-conductive substrates to be probed,[6] it is not strictly necessary for conductive (electrode) surfaces, as demonstrated in recent studies,[11,12,21] where a simplified single-channel configuration based on a fine nanopipet (diameter as small as 30 nm) was employed to perform high-speed, high-resolution synchronous topographical/electrochemical activity mapping. These studies build on the earlier approach of using a simple single-channel nanopipet tip for meniscus-based electrochemical imaging.[2]

In this contribution, we consider the use of SECCM in chronopotentiometric (galvanostatic) mode with a single-channel nanopipet probe. Despite being less used than controlled-potential methods in modern electrochemical science, controlled-current or galvanostatic techniques still play an important role in diverse fields, including coatings (*i.e.*, electroplating)[22] and battery research,[23] where constant-current conditions are usually applied to allow fine control over the rate of (electro)chemical processes. For instance, a notable advantage of galvanostatic techniques in electroplating is that the charge-passed, and hence the amount of material electrodeposited can be controlled precisely, which generally makes it easier to obtain a uniform deposition compared to constant-potential conditions.[24] Another interesting application of galvanostatic methods can be found in the field of electrocatalysis, where a commonly adopted metric for benchmarking the activity of a material is the overpotential required to achieved a given current density (*e.g.*, 10 mA cm^{-2}, η_{10});[25,26] as explored herein, this kind of determination is conceptually easier under controlled-current conditions, rather than controlled-potential. Galvanostatic SECCM has recently been used as part of studies to map the charge/discharge characteristics of battery electrodes;[21,27,28] and these and further applications bring a need to understand in more detail the electrochemical response of this imaging mode.

Herein, chronopotentiometric SECCM has been applied for the study of three model electrochemical systems, in order to verify the method. Firstly, the outer-sphere

$[Ru(NH_3)_6]^{3+/2+}$ process was characterized at a polished glassy carbon (GC) surface, where ideal electrochemical reversibility (*i.e.*, "Nernstian" behavior) is expected, given the scale of the nanopipet used (*ca.* 500 nm) compared to the structural heterogeneity in GC (*i.e.*, it is microstructurally isotropic[29]). These measurements sought to confirm the stability of the meniscus (droplet) cell and demonstrate the reproducibility of the electrochemical potential (*E*) - time (*t*) curves at the different pixels among the thousands of an SECCM scan. Secondly, the same process was investigated on an aged highly-oriented pyrolytic graphite (HOPG) surface, which has previously been shown to exhibit complex, structure-dependent (*i.e.*, edge plane, vs. basal plane) electron-transfer properties under these conditions.[6] Finally, the technique was employed in the context of electrocatalysis to probe the hydrogen evolution reaction (HER) activity of bulk MoS_2, demonstrating enhanced catalytic activity at macroscopic defect sites where the edge plane is exposed.

Experimental

Chemical reagents and electrode materials. Perchloric acid ($HClO_4$, Sigma-Aldrich, 70%), potassium chloride (KCl, Sigma-Aldrich), hexaammineruthenium(III) chloride ($[Ru(NH_3)]Cl_3$, Sigma-Aldrich), dichlorodimethylsilane [$Si(CH_3)_2Cl_2$, Acros Organics, ≥ 99%] were used as supplied by the manufacturer. All solutions were prepared with deionized water (Integra HP, Purite, U.K.), which had a resistivity of 18.2 MΩ.cm (25°C).

The glassy carbon (GC) substrate was purchased from HTW-Germany and polished with an aqueous suspension of Al_2O_3 (Buehler, U.S.A.), of particle size 0.05 μm, before use. The HOPG sample originated from GE Advanced Ceramics (U.S.A.) and was a gift from Prof. R. L. McCreery, University of Alberta, Canada. Full characterization of this material, including the step edge density, has been reported.[30] The sample was fixed to an aluminum scanning

electron microscopy (SEM) stub with conductive silver paint (RS Supplies, U.K.). Prior to use, the HOPG crystal was gently cleaved using the "scotch tape method"[31] and subsequently left exposed to air for 1 hour, to allow surface "aging". The molybdenite (MoS_2) crystal (semiconducting 2H phase, as characterized previously[13]) was purchased from Manchester Nanomaterials (U.K.). Prior to use as an electrode material, the MoS_2 crystal was fixed on a glass microscope slide with carbon SEM tape and mechanically cleaved using the "scotch tape method".[31] To ensure electrical connection and in order to avoid ohmic resistance through the material, the cleaved MoS_2 surface was electrically connected through a top contact with conductive copper SEM tape.

The Ag/AgCl quasi-reference counter electrode (QRCE) was prepared by anodizing an annealed silver wire (0.25 mm diameter, Goodfellow, U.K., 99.99%) in a saturated KCl solution. The QRCE was then calibrated potentiometrically (measuring the open circuit potential for approximately 10 min) in the solution of interest (5mM $[Ru(NH_3)_6]Cl_3$ + 10 mM KCl) against a commercial 3.4 M Ag/AgCl electrode (ET072, eDAQ, Australia), which has a standard potential of +205 mV vs. the normal hydrogen electrode (NHE).[32] The Pd/H_2 QRCE was prepared by electrochemical dissolution of H_2 in annealed palladium wire (0.25 mm diameter, Goodfellow, U.K., 99.99%). To achieve this, the Pd wire was held in a 0.1 M $HClO_4$ solution at -3 V vs. Pt wire for 30 mins, and used for experiments immediately after. All the experiments involving the $[Ru(NH_3)_6]^{3+/2+}$ process employed the Ag/AgCl QRCE, while for the HER on MoS_2 the Pd/H_2 QRCE was employed.

Surface characterization. Scanning electron microscopy (SEM) was employed to characterize the nanopipet probe geometry and electrode surfaces (HOPG and MoS_2) after SECCM experiments, as previously reported.[6,33,34] The SEM images were obtained on a GeminiSEM 500 scanning electron microscope (Zeiss, Germany), at an acceleration voltage of 5 kV using an InLens detector.

Electrochemical measurements. All experiments in the SECCM configuration were performed on a homebuilt scanning electrochemical probe microscopy (SEPM) workstation, as previously described,[17] with salient details given below. The fundamental instrumentation for galvanostatic SECCM is comprised of an *x*-*y*-*z* piezoelectric positioner ((P-621.2CD with E-625 Controller for *x*-*y* and P-753.3CD with E-665 controller for *z*, Physik Instrumente, Germany), a galvanostat (home-built herein, also functioned as a voltage follower), a waveform generator (digital herein, utilized for applying the desired current to the galvanostat) and a data collection system (FPGA card herein). A schematic representation of the setup for galvanostatic SECCM and chronopotentiometric measurements is given at the start of the results and discussion section (Figure 1).

The nanopipet probe consisted of an electrolyte-filled single-channel nanopipet, obtained by pulling a borosilicate glass capillary (30-0044, GC120F-10, Harvard Apparatus, U.K.) to a sharp tip with a commercial CO_2 laser puller (P-2000, Sutter Instruments, U.S.A.). Pulling parameters can be found in the Supporting Information, Section S.1. After pulling, the probes were silanized by dipping them into $Si(CH_3)_2Cl_2$ with argon flowing through the tip (at a pressure of 6 bar) for 1 min (this prevented the silane from entering the tip). This procedure created a hydrophobic surface on the outside of the tip, which aided meniscus cell confinement during scanning (note that silanization was only performed on probes that were >200 nm in diameter). The probe was then filled with the electrolyte solution of interest, and a silicone oil layer was added on the top of the solution in the tip to minimize evaporation during prolonged scanning. The QRCE (Ag/AgCl or Pd/H_2, as described above) was placed inside from the back, and positioned *ca.* 3 cm from the tip end.[35] The nanopipet was subsequently mounted on the z-piezoelectric positioner and moved into the initial position by the use of coarse micropositioners (*x*-*y*-*z* movement), while the sample was mounted on the *x*-*y* piezoelectric positioner.

The chronopotentiometric SECCM experiments were performed with a "hopping mode" imaging protocol, as previously described.[18,19] This protocol involved approaching the nanopipet probe to the substrate surface at a series of predefined locations in a grid and, upon each meniscus landing (note that the pipet itself did not contact the surface), a chronopotentiometric measurement was made, allowing the creation of time-dependent 2-dimensional electrochemical potential "maps" of the substrate. In addition, the *z*-position of the probe was recorded synchronously on every approach, and the contact *z*-coordinate was plotted as a function of *x*-*y* coordinate to create a topographical map of the substrate surface. During approach of the tip, the potential measured in the galvanostat circuit was employed for positional feedback in order to detect meniscus contact with the surface. A change of 6 V from the 'overload' value (±10 V) experienced when the tip was at open circuit (tip away from the surface) was set as the feedback threshold to indicate meniscus contact and to immediately stop the nanopipet movement on each approach. The nanopipet speeds were 3 μm s^{-1} on approach, 20 μm s^{-1} on retract (by 4 μm) and 5 μm s^{-1} for lateral movement. The distance between each pixel depended on the tip size and sample; pixel densities are specified for each data set presented.

The entire SEPM configuration was placed on a passive mechanical vibration isolator platform (Minus K® Technology, Inc. U.S.A.), which was located in an aluminum faraday cage equipped with heat sinks and acoustic foam in order to minimize mechanical vibration, electrical noise and thermal drift. The current (i_{app}) was applied at the QRCE and potential (E_{surf}) was measured at the substrate (working electrode) with a home-built galvanostat (see Supporting Information, Section S.2 for further information). The corresponding output potential was measured every 4 μs, which was averaged 129 times, to give a data acquisition rate of 516 μs per point. All data acquisition and instrumental control was carried out with an FPGA card (PCIe-7852R) controlled by a LabVIEW 2016 (National Instruments, U.S.A.)

interface running the Warwick Electrochemical Scanning Probe Microscopy software (WEC-SPM, www.warwick.ac.uk/electrochemistry).

After collection, all the raw data were processed using the Matlab R2016b (Mathworks, U.S.A.) software suite. "False approach" points, *i.e.* where the nanopipet was triggered to stop but subsequent analysis revealed that meniscus contact had not been made (evident from a 'spike' in the synchronously obtained topographical map, see supporting information, Figure S3c), were discarded. These events were rare, *e.g.* amounting to 12 out of the 6561 pixels for $[Ru(NH_3)_6]^{3+/2+}$ process on GC, discussed below. Non-linear sample tilt and drift in topographical maps was corrected using the scanning probe image processing (SPIP) software package (v. 6.0.14, Image Metrology, Denmark). Data plotting was performed with the OriginPro 2016 64bit (b9.3.226, OriginLab, U.S.A.) and Matlab R2016b (for the 2D maps) software packages. All topographical and electrochemical maps were plotted without any data interpolation.

Results and Discussion

Chronopotentiometric SECCM: working principles. A general scheme of the technique and typical data for a single pixel are shown in Figure 1. As the single channel nanopipet (Figure 1a) was moved across the surface in the "hopping-mode" regime, the measured galvanostat output potential (E_{output}) was used for positional feedback (*vide supra*). Figure 1b shows representative examples of the *z*-position of the probe, current applied by the galvanostat (i_{app}) and E_{output} for a single "hop" with a single pulse chronopotentiometry measurement (preceded by a landing at open circuit potential, OCP), as used for the $Ru(NH_3)_6^{3+/2+}$ case discussed below. When i_{app} of a specific magnitude and polarity is set at the galvanostat, the instrument tunes E_{output} (equivalent to E_{surf} during meniscus contact) until the set current is reached. If the electrochemical cell has not been formed (*i.e.*, meniscus contact has not been made with the surface, 'non-contact'), E_{output} will be in the 'overload' state [±10 V for our instrument, with the sign dependent on the polarity of i_{app}, *i.e.*, Figure 1b, **(1)**]. E_{output} remains constant at the 'overload' value until the probe makes meniscus contact with the surface (note that the probe itself does not make physical contact with the surface). This was true even when the current was set to 0 pA during the nanopipet approach, as in Figure 1b, **(1)** and **(2)**. Once meniscus contact was sensed, E_{output} quickly transitioned to E_{surf} [*i.e.*, Figure 1b, **(2)**]. This dramatic potential change (several volts) was set as the "feedback threshold" for stopping the *z*-approach of the probe, and starting the chronopotentiometric pulse experiment at a time 0.5 s later. The probe was kept standing at that fixed distance from the surface for the whole duration of the chronopotentiometric analysis (*i.e.*, during a single hop), with no feedback during the contact period, as the thermal drift of the system (approximately 0.1 nm/s) was considered to be negligible on the time scale of a single hop of the scan, as assessed in our previous work.[36]

In Figure 1b, **(3)** the current was pulsed to 23 pA (see next section for clarifications about the amplitude of the current) and the corresponding potential measured as a function of time. After

the chronopotentiometric pulse (duration 1.5 s in Figure 1), the probe was retracted a fixed distance (2 μm) from the surface [*i.e.*, Figure 1b, **(4)**], before being moved to the next point and E_{output} again adopted the 'overload' condition [*i.e.*, Figure 1b, **(5)**]. During the retraction, i_{app} was pulsed to a larger value [*e.g.*, 30 pA in Figure 1, **(4)**], in order to minimize the time taken for E_{output} to reset to the non-contact or 'overload' value (*i.e.*, ±10 V) for the next hop [*i.e.*, $dV/dt \propto 1/i_{app}$ in Figure 1, **(4)**].

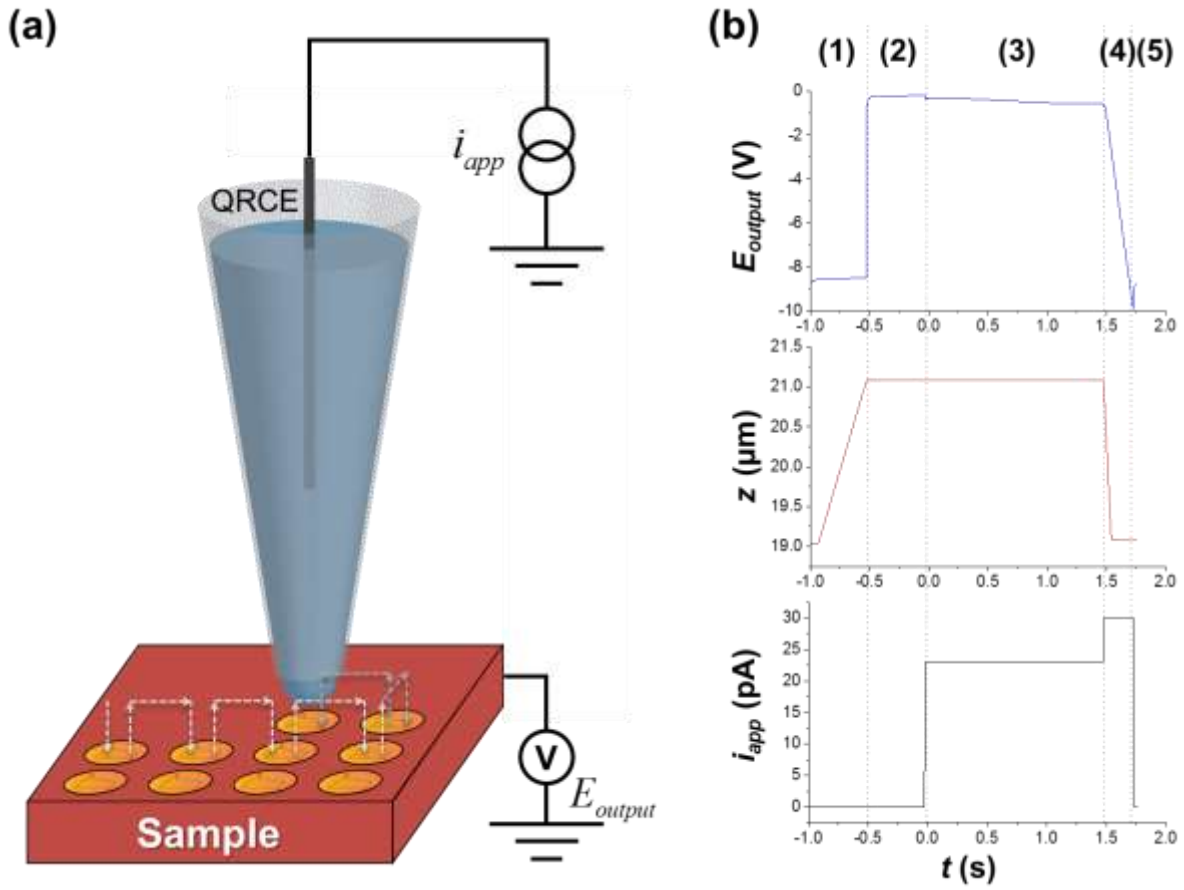

Figure 1: (a) Schematic of the SECCM configuration deployed in the galvanostatic mode with a single channel pipet probe. The arrows indicate the movement of the probe across substrate (working electrode) surface during a typical scanning protocol. **(b)** Plots showing the variation of three main parameters (*z*-position of the tip, applied current i_{app}, and output potential of the galvanostat, E_{output}) recorded synchronously during a single hop of a typical scanning experiment. Each individual operation is marked with a number: (1) approach; (2) meniscus contact; (3) current pulse to desired value; (4) retract (second current pulse to establish 'overload condition' and; (5) movement to the next point. These data were collected under the following experimental conditions: tip diameter

ca. 400 nm (tip orifice area *ca.* $1.2 \cdot 10^{-9}$ cm^2), electrolyte solution 5 mM $[Ru(NH_3)_6]Cl_3$ in 10 mM KCl, performing the $[Ru(NH_3)_6]^{3+/2+}$ process on a GC substrate.

This methodology, combined with the use of nanopipets of different sizes (ranging from 150 nm to 800 nm in diameter) has been employed to perform spatially-resolved chronopotentiometric measurements in a range of electrochemical systems (*vide supra*) in order to demonstrate the versatility and wide applicability of the chronopotentiometric SECCM technique.

$[Ru(NH_3)_6]^{3+/2+}$ on glassy carbon: stability and reproducibility of the confined electrochemical cell. The $[Ru(NH_3)_6]^{3+/2+}$ electron transfer reaction is a rapid, mechanistically simple, outer-sphere process:[37]

$$[Ru(NH_3)_6]^{3+} + e^- \rightleftharpoons [Ru(NH_3)_6]^{2+},\ E^0 = -0.208\text{V vs. Ag/AgCl (sat. KCl)} \quad (1)$$

It is well-known to exhibit the characteristics of an ideal, reversible (*i.e.*, mass-transport controlled) process at most electrode materials, including GC under 'typical' DC cyclic voltammetric conditions.[38] Thus, this Nernstian process was investigated first at a GC electrode in order to examine the reproducibility of galvanostatic SECCM.

A typical chronopotentiometric curve for a Nernstian process would present a plateau at a potential close to $E^{0'}$ followed by a dramatic change of E at a time $t = \tau$, described by the Sand equation:[39]

$$\tau = \frac{(nFC^*)^2 D\pi}{4(j_{app})^2}, \quad (2)$$

where j_{app} is the applied current density, C^* is the bulk concentration of the redox species, D is its diffusion coefficient, n is the number of electrons and F is the Faraday constant. At such time, the concentration of the electroactive species tends to 0 at the electrode surface. A

summary of the theoretical principles of chronopotentiometry, as well as examples of *E-t* curves obtained at a macrodisk electrode (Figure S2) are included in the Supporting Information, Section S.3.

It has previously been established that radial diffusion makes a significant contribution to mass-transport in the SECCM configuration. As a rule of thumb, the diffusional flux in SECCM is *ca.* 10% of that expected at the same size microdisk electrode,[34] confirmed herein by performing linear sweep voltammetric experiments, as shown in the Supporting Information, Section S.4, Figure S3a. A near steady-state voltammogram is obtained at a scan rate of 100 mV s^{-1}, with the steady-state limiting cathodic current (i_{ss}) determined to be 24 pA (j_{ss} = 13.3 mA cm^{-2}, given a radius of SECCM contact, a, of 2.5 × 10^{-5} cm estimated by the cross-sectional area of the tip end), which is approximately 15 times smaller than the value expected at the same sized microdisk ($i_{ss}=4nFDC^{*}a$).[40] Analogous to the case with microdisk electrodes, where radial diffusion needs to be accounted for, the diffusion equation under galvanostatic conditions does not have an analytical solution and the potential-time behavior is highly dependent on i_{app}, particularly in relation to i_{ss}.[41-43] If $i_{app}/i_{ss} \gg 1$, the approximate solution for τ can be obtained from equation (2), resulting in a macroelectrode-like response, whereas if i_{app} approaches i_{ss}, the transition time will tend to infinity, with the concentration of electroactive species adopting a constant, non-zero value at the electrode surface, and a steady-state diffusion regime established.

This predicted behavior was verified in the SECCM configuration by performing chronopotentiometric experiments at a series of i_{app}, as shown in Figure 2. In all cases, the current was pulsed from an initial value i_{app} = 0 pA (*i.e.*, close to OCP) to a particular cathodic current value (ranging in magnitude from 25 to 31pA). These values were all larger than i_{ss} = 24 pA in order to see the transition. Typical chronopotentiometric curves are shown in Figure 2a. For clarity, the meniscus landing response with 0 pA current is set to negative times and

the cathodic pulses start at t = 0 s. Immediately after the cathodic current pulse, in all curves, E_{surf} presents a very sharp negative 'spike', before settling at the expected value for the reduction process (assuming a reversible process, see Supporting Information, Section S.4) on the millisecond timescale. This potential 'spike' can be attributed to double layer charging and stray capacitance as i_{app} is changed abruptly. As shown in Figure 2b, τ becomes much extended as i_{app} approaches i_{ss}, analogous to the case with microdisk electrodes.[41-43] Conversely, τ approaches a more linear behavior with respect to j^{-2} at higher values of i_{app} (shown in Figure 2b), analogous to the case with macroscale electrodes (*vide supra*).

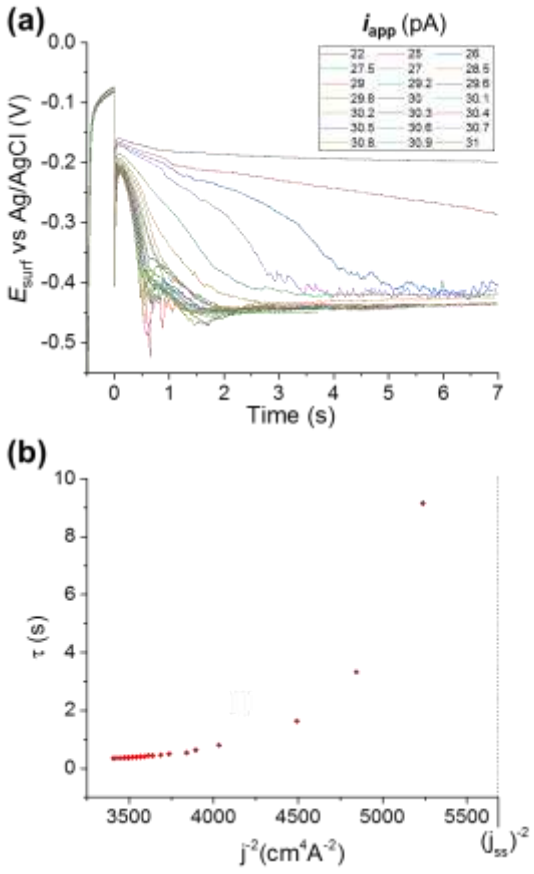

Figure 2: (a) Single-pulse galvanostatic curves obtained in the SECCM configuration with a solution containing 5 mM $Ru(NH_3)_6^{3+}$ and 10 mM KCl at a GC substrate. For times, t < 0 s, i_{app} = 0 pA and the current transient corresponds to the landing of the meniscus. At t = 0 s, i_{app} was jumped to a value in the range 22 to 31pA for the cathodic pulse (positive times, indicated on the plot). **(b)** Plot of transition time, τ [calculated from the data in **(a)**]

versus j^{-2}. The vertical dotted line in (b) indicates the inverse square of the steady-state current density (i.e., j_{ss}^{-2}), for j_{ss} = 13.3 mA cm^{-2}. In these experiments, the diameter of the nanopipet probe was *ca.* 480 nm.

It should be noted that the transition becomes broader and less well-defined with decreasing i_{app} (see Figure 2a), making it difficult to accurately determine τ. In addition, comparison with theory[41-43] reveals that the values of i_{app} employed herein (up to 31 pA) are too low to observe fully linear τ vs. j^{-2} behavior (*i.e.*, as predicted by the Sand equation), but it was difficult to apply higher current values, as τ becomes too small in comparison to the timescale of double layer and stray capacitance charging (*vide supra*). For this reason, no further attempt was made to treat the τ vs. j^{-2} data quantitatively. Finally, it is interesting to note that after the transition, as shown in Figure 2a, the *E-t* curves obtained in the SECCM configuration become relatively noisy and unstable, if compared to the corresponding ones obtained on a macrodisk electrode (see Supporting Information, Figure S2a). This is probably due to slight instability of the droplet (meniscus) cell during the cathodic process to which the potential transitions (*i.e.*, oxygen reduction and/or HER).

In order to test the reproducibility of the galvanostatic method for long timescale imaging (≈5 hours), a scan consisting of 6561 individual *E-t* experiments (81 × 81 points, square grid, hopping distance of 1 μm) was carried out on a polished GC electrode. A cathodic chronopotentiometry pulse with i_{app} = 23 pA ($j_{app} \approx$ 15 mA cm^{-2}) was performed at every point, preceded by 0 pA applied current for meniscus landing on the surface (*i.e.* OCP), with i_{app} chosen to be high enough in relation to i_{ss} to observe the transition (note, the probe used in these experiments was smaller than that used above in Figure 2, around 450 nm of diameter, and i_{ss} was lower than the previous probe). Figure 3a plots the average of all recorded *E-t* curves, with a representation of the statistical tolerance at every point. Evidently, the curves are very reproducible prior to the transition ($0 < t < \tau$, *i.e.*, during the $[Ru(NH_3)_6]^{3+/2+}$ process), confirming that the meniscus cell (footprint) is very stable and consistent on this timescale.

The first section of the curve ($0 < t < \tau$) was fitted with a typical macroscale potential profile for a Nernstian process [eqn. (S4), Supporting Information] to give values of τ and $E_{\tau/4}$ (equal to $E^{0'}$, assuming $D_{[Ru(NH_3)_6]^{3+}} = D_{[Ru(NH_3)_6]^{2+}}$, as explored in the Supporting information, eqn. S5), of 0.502s ± 0.001s and -0.199V ± 0.002V vs. Ag/AgCl (3.5 M KCl), respectively. In particular, $E_{\tau/4}$ exhibits a very narrow Gaussian distribution, with a standard variation of just σ = 0.002V, a testament to the reproducibility of this methodology and the meniscus contact at thousands of different points across the working electrode surface. This is further evident from an analysis of the drift of $E_{\tau/4}$ over the scan time (Figure 3b), which changes by only *ca.* −5 mV over the 5 hour timescale, likely attributable to slight drift in the QRCE potential, as previously reported.[35] Finally, an analysis of the $E_{\tau/4}$ map and topography image does not indicate any substantial variation during the scan, as shown in the Supporting Information, Figure S3b.

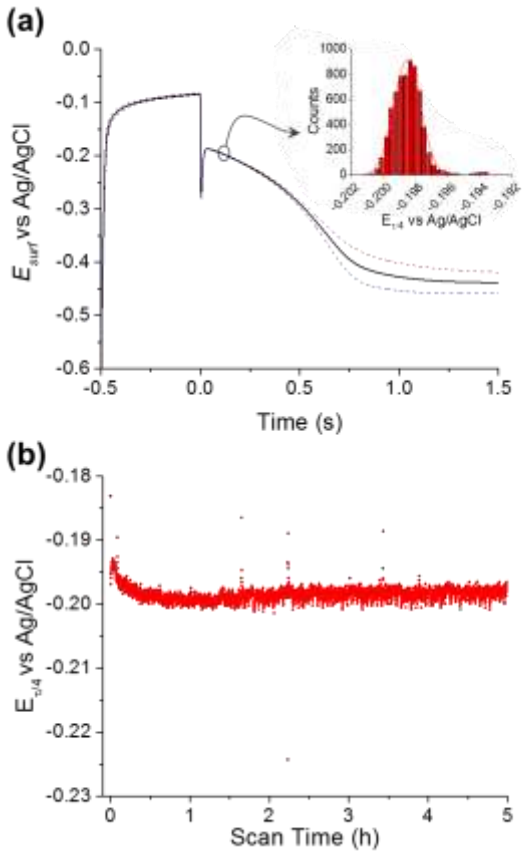

Figure 3: (a) Average *E*-*t* curve (N = 6561) obtained from an 81 × 81 pixel galvanostatic SECCM scan. At each pixel, meniscus landing was achieved with i_{app} = 0 pA (OCP) and the current was stepped to i_{app} = 23 pA during the cathodic current pulse (set at t = 0 s). The standard deviation from measurements at all points is also shown (dotted lines), as well as the statistical analysis of $E_{\tau/4}$ (inset). (b) Variation of $E_{\tau/4}$ measured over the *ca.* 5 hour scan time. In these experiments, the diameter of the nanopipet probe was *ca.* 400 nm.

Overall, these results verify the general applicability and reproducibility of SECCM chronopotentiometry, which is expanded to more complex electrochemical systems in the following sections.

$[Ru(NH_3)_6]^{3+/2+}$ on aged HOPG: visualizing structure-dependent activity on a heterogeneous surface. Previous work employing SECCM in tandem with complementary microscopy/spectroscopy techniques showed that for the $[Ru(NH_3)_6]^{3+/2+}$ process on "aged" HOPG (exposed to the ambient atmosphere for an extended period before measurements), there was a difference in the $[Ru(NH_3)_6]^{3+}$ reduction potential between the basal surface and step edge sites, with enhanced electrochemical activity at step edges.[6] Thus, the $[Ru(NH_3)_6]^{3+/2+}$ process on aged HOPG was investigated as a model system to demonstrate the capability of SECCM chronopotentiometry for highlighting (and quantifying) differences in electrochemical activity on a heterogeneous surface. A chronopotentiometric scan (961 individual experiments, 31 × 31 points in a square grid, with a hopping distance of 2 μm) was performed on a mechanically-exfoliated HOPG substrate that had been aged for 1 hour prior to use. In these experiments the cathodic current, j_{app} = 1.5 mA cm^{-2} (i_{app} = 10 pA), was selected to be only *ca.* 15% of j_{ss} ($j_{ss} \approx$ 10 mA cm^{-2}) as the aim was to quantify the activity for the $[Ru(NH_3)_6]^{3+/2+}$ process, and so measuring τ was not necessary. In addition, a relatively long pulse time of 3 s was employed in order to ensure the electrochemical process achieved steady state (*vide supra*).

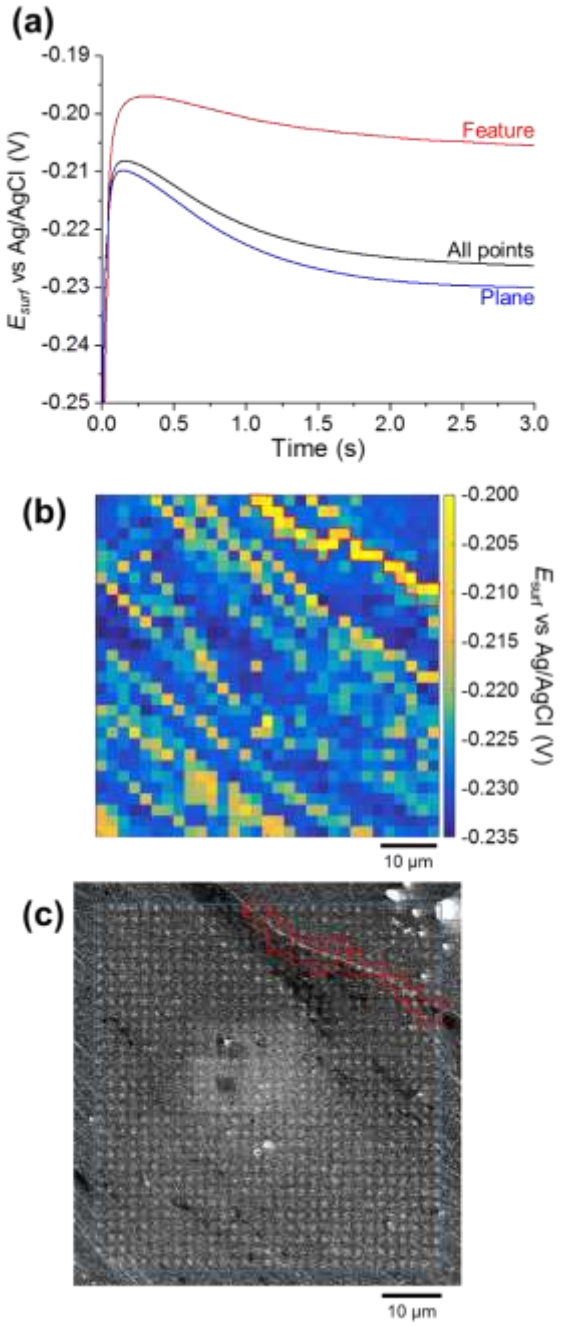

Figure 4: (a) *E-t* plots for the reduction scan of 5 mM $[Ru(NH_3)_6]^{3+}$ (10 mM KCl supporting electrolyte) on an aged HOPG surface. The plots were obtained by averaging: all points of the scan (black trace); points obtained on the step edge feature [red trace, indicated by the red boxes in **(b)** and **(c)**]; and points obtained at the basal surface (blue trace). All curves were measured with i_{app} = 10 pA, which was maintained consistently throughout the experiment (*i.e.*, during each approach and landing). In these experiments, the diameter of the pipet probe was *ca*. 800 nm. **(b)** Map showing E_{surf} at t = 3s. **(c)** SEM image of the same area, with the scan area marked by the blue square.

A summary of key results is shown in Figure 4. Figure 4a shows the average of all the galvanostatic curves (N = 961) collected on the aged HOPG surface. In agreement with the results above, the *E-t* curve initially exhibits a sharp negative spike on the millisecond timescale (charging) before settling on the expected waveshape for this kind of system, *i.e.* a plateau with an E_{surf} value close to (but not equal to) E^0, as discussed earlier. A spatially-resolved electrode potential map of the HOPG surface was constructed by plotting E_{surf} measured after 3 s vs. *x-y* position, as shown in Figure 4b. Clearly, the basal surface possesses relatively uniform activity (blue areas in the map), with a series of "high activity" features running diagonally across the scan area, revealed to be step edges through co-located imaging with scanning electron microscopy, SEM (image shown in Figure 4c). Note that these features were too small to identify from the SECCM topographical map recorded synchronously with the electrochemical data, which just appeared as a relatively flat and featureless surface (not shown), due to the size of the pipet probe used (*vide supra*). The most prominent feature (likely the largest multilayer step edge), set in the top right corner of the scan area exhibits a potential that is, on average, 21 mV more positive than the one of the surrounding plane (ranging from +13 mV at the beginning to +24 mV at the end of the pulse), indicating that the electrochemical reaction proceeds more readily at the step edge, for reasons outlined in detail elsewhere.[6]

HER on MoS_2: basal vs. edge plane activity. MoS_2 is a promising low-cost, earth-abundant electrocatalyst for the HER.[44,45] The sample used herein was naturally occurring molybdenite (2H phase), a layered crystalline semi-conductor with a surface consisting of extended basal planes interrupted by edge plane defects of variable height (monoatomic to several multi-layer, tens of nm in size). It is generally accepted that the basal plane of MoS_2 (2H phase) is a relatively inactive HER catalyst, while the edge plane possesses high catalytic activity, established from theoretical and experimental standpoints.[25,46] Indeed, recent voltammetric SECCM studies mapped the electrocatalytic activity of molybdenite, revealed uniform

electrocatalytic activity at the basal plane (on the μm lengthscale) and enhanced activity at the edge plane.[11,13]

As alluded to above, chronopotentiometry presents a very facile route for benchmarking catalytic materials *(i.e.*, determining the overpotential required for a given current density, at particular locations of the surface, with high spatial-resolution). Besides, it allows the measurement to be carried out at a very small current density (*i.e.*, the "foot of the wave", where the reaction is purely surface-controlled) compared to the current densities that are generally measured in potential-controlled methods, thus opening up a new dynamic (lower current density) range for electrocatalytic imaging, as will be demonstrated here. For these measurements a current density of 2 mA cm^{-2} (i_{app} = 0.628 pA, with a 150 nm diameter probe, assuming that the wetted area is the same size as the probe dimensions, as previously reported[13]) was used on a mechanically exfoliated MoS_2 crystal in 0.1 M $HClO_4$; a pulse of 0.5s was applied to every point, giving an average rate of acquisition of 0.75s per point (taking into account the time of approach, retract and lateral movement), which is comparable with the scan rate achieved in potential-controlled SECCM work on the same system.[11]

The main results of the chronopotentiometric scan are shown in Figure 5. The topographical map shown in Figure 5a, constructed directly from the *z*-approach data collected during the SECCM experiment, reveals that the scan area is predominantly on the basal plane, with large, multilayer step edges (tens of nm in size) present in the top-left and top-right corners. Comparing the topographical map with the spatially-resolved chronopotentiometric map (constructed at 0.3 s, where the curve stabilizes) in Figure 5b confirms the aforementioned heterogeneity between the basal and edge planes, with more positive potentials (*i.e.*, smaller overpotentials) measured at the latter. As shown in Figure 5c, line-scan profiles of *z*-height and E_{surf} further demonstrate that the sites of enhanced activity are located on the multistep surface features (*i.e.*, defects sites where the edge plane is exposed).

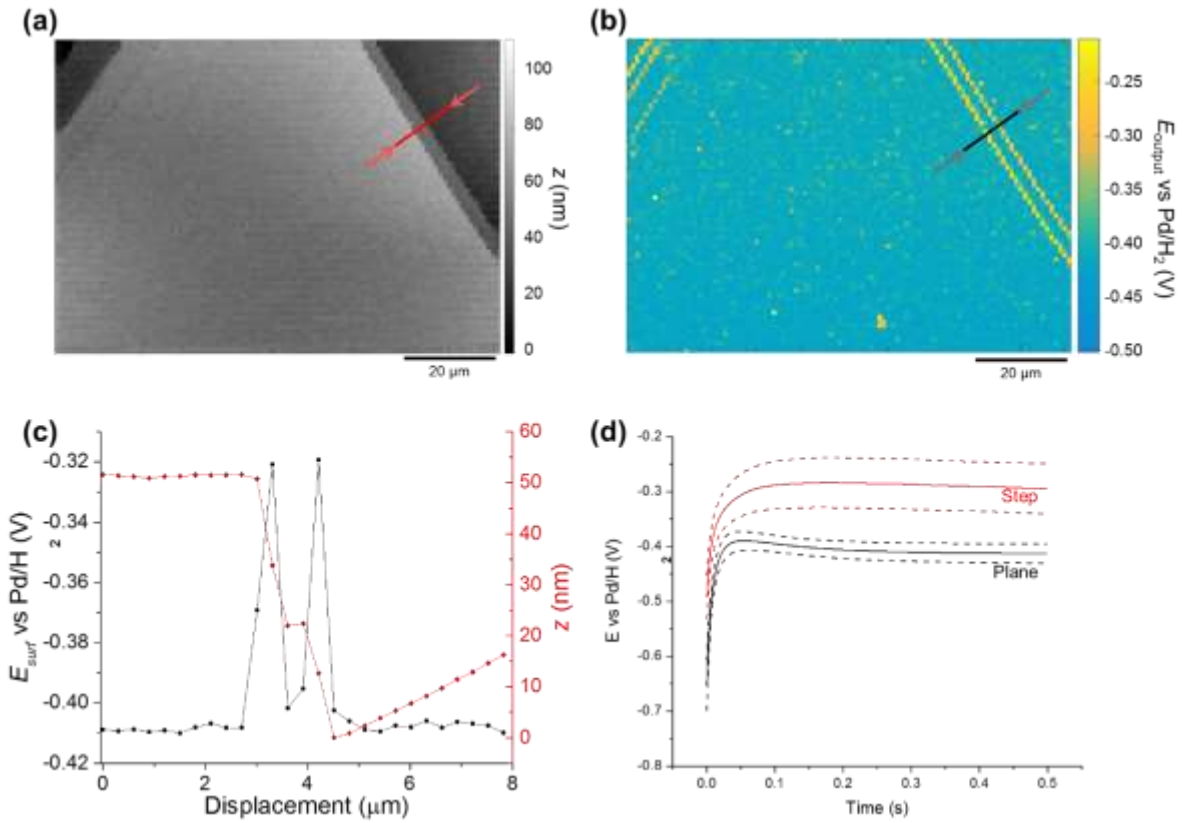

Figure 5: SECCM **(a)** topographical and **(b)** galvanostatic (E_{surf} at 0.3 s) electrochemical activity maps obtained from 0.1 M $HClO_4$ solution, visualizing HER activity at the surface of MoS_2. **(c)** Line scan profiles of topography (red trace) and E_{surf} (black trace), obtained at the lines indicated in **(a)** and **(b)**, respectively. **(d)** Average *E-t* curves obtained at the basal plane (black trace) and two step-edge features located in the top-right corner of the scan area (red trace). Standard deviations are also represented (dashed lines). In these experiments, the diameter of the nanopipet probe was *ca.* 150nm.

Average *E-t* curves shown in Figure 5d reveal that the basal plane possesses a uniform activity on this length scale, with an average E_{surf} of -413 mV ± 18 mV vs. Pd/H_2 at the end of the pulse. In addition, the average E_{surf} taken from the two large features located on the top-right of the map (see Figure 5d, red solid line) is -295 mV ± 46 mV vs. Pd/H_2, again demonstrating accelerated HER kinetics at the exposed edge plane. It is worth noting that the red *E-t* curve arises from an area comprised of both basal and edge plane, with the size of the feature determining the basal:edge ratio in the probed area (*i.e.*, the edge plane activity was not measured in isolation). This is why the activity enhancement (evidenced by the shift in E_{surf})

scales with step size, with bigger steps appearing to be being more active than the smaller ones, down to monolayer levels (*e.g.*, see the Supporting Information, Figure S4). Given that the geometry of the step-edge features are known from the topographical map, edge plane activity could be estimated directly, following the procedure similar to that outlined in our previous work,[13] although this was not of interest here.

It is worth remarking that analysis carried out above has allowed catalytic activity to be probed directly by simply applying a current of 0.628 pA (*ca.* 2 mA cm^{-2}), which is considerably lower than the average currents measured with the voltammetric (*e.g.*, controlled-potential) techniques utilized in previous studies (up to -1v VS RHE and 60pA with a 50nm diameter tip).[9,13,14,21] Compared to a typical SECCM linear sweep voltammetry experiment (LSV), such current and potentials will fall in the very early foot of the reduction wave, where the distinction between the activity of planes and edges is quite difficult due to the current being very close to noise level of the current. This is one major advantage of the galvanostatic approach, as this and similar analyses can be carried out without significantly polarizing the substrate (working electrode) surface.

Conclusions

SECCM was deployed in the controlled-current (galvanostatic or chronopotentiometric) mode to interrogate electrochemical systems of increasing complexity. Firstly, the analysis of the electrochemically reversible $[Ru(NH_3)_6]^{3+/2+}$ process at a homogeneous surface (on the scale of the SECCM probe), polished GC, demonstrated that the meniscus cell configuration is sufficiently stable when operated in the controlled-current mode, with a consistent electrochemical response ($E_{\tau/4}$ = −0.210 ± 0.002 V vs. Ag/AgCl) recorded over an extended experimental timescale (over 5 hours, and over 6000 individual measurement points). Further

analysis of the same process on an aged HOPG surface revealed that subtle differences in activity, with enhanced activity of the edge plane relative to the basal plane (*ca.* 20 mV difference in E_{surf}), could be detected readily with high sensitivity. Finally, the optimized setup was applied to study the activity of an electrocatalytic surface, proving the efficacy of galvanostatic techniques for "benchmarking" catalytic activity by measuring the overpotential at a given current density. Enhanced catalytic activity towards the HER was measured at the edge plane of MoS_2 relative to the basal plane revealed directly by comparing the synchronously obtained E_{surf} and topographical "maps". Remarkably, high sensitivity and resolution were achieved in both the topographical and electrochemical images, despite the application of a very small current (< 1 pA), avoiding significant polarization or damage of the sample. It follows that this approach should allow the study of the surface dependency of processes that would be difficult to examine in controlled-potential mode, due to the occurrence of other higher current processes at nearby potentials, such as for example, the ubiquitous interference of the HER with electrochemical CO_2 reduction (ECR) in aqueous electrolytes.[47,48] This is also an important consideration, for example, in the study of corrosion-related processes, where small changes in potential can change the active dissolution current by orders of magnitude, resulting in significant damage to the material under examination. This avenue will be explored further in future work.[49] Overall, the work presented here opens up promising new applications of galvanostatic techniques at the nanoscale level, including to fields where controlled-current methods are typically applied, such as electroplating or energy storage materials characterization, and where the high spatial resolution of SECCM could be very powerful in elucidating structure-activity correlations.

Associated Content

Supporting information

Nanopipet pulling parameters, scheme of the homebuilt electronic equipment of chronopotentiometric measures, supplementary theory for chronopotentiometry at macroscale and additional SECCM images. This material is available free of charge via the Internet at http://pubs.acs.org.

Author Information

Corresponding Authors

*C.Bentley.1@warwick.ac.uk (C.L.B.), P.R.Unwin@warwick.ac.uk (P.R.U.)

Notes

The authors declare no competing financial interest.

Acknowledgements

E.D. acknowledges Lubrizol Ltd. and Warwick Collaborative Postgraduate Research Scheme for funding. C.L.B. acknowledges financial support from the Ramsay Memorial Fellowship Trust. P.R.U. gratefully acknowledges support from a Royal Society Wolfson Research Merit Award. The authors thank Dr. Minkyung Kang for helpful discussions and assistance with the initial galvanostatic SECCM set up.

References

(1) Ebejer, N.; Schnippering, M.; Colburn, A. W.; Edwards, M. A.; Unwin, P. R. *Anal. Chem.* **2010**, *82*, 9141-9145.

(2) Williams, C. G.; Edwards, M. A.; Colley, A. L.; Macpherson, J. V.; Unwin, P. R. *Analytical Chemistry* **2009**, *81*, 2486-2495.

(3) Bentley, C. L.; Kang, M.; Unwin, P. R. *J. Am. Chem. Soc.* **2019**, *141*, 2179-2193.

(4) Bentley, C. L.; Edmondson, J.; Meloni, G. N.; Perry, D.; Shkirskiy, V.; Unwin, P. R. *Analytical Chemistry* **2019**, *91*, 84-108.

(5) Byers, J. C.; Güell, A. G.; Unwin, P. R. *J. Am. Chem. Soc.* **2014**, *136*, 11252-11255.

(6) Güell, A. G.; Cuharuc, A. S.; Kim, Y.-R.; Zhang, G.; Tan, S.-y.; Ebejer, N.; Unwin, P. R. *ACS Nano* **2015**, *9*, 3558-3571.

(7) Unwin, P. R.; Güell, A. G.; Zhang, G. *Accounts of Chemical Research* **2016**, *49*, 2041-2048.

(8) Chen, C.-H.; Meadows, K. E.; Cuharuc, A.; Lai, S. C. S.; Unwin, P. R. *Phys. Chem. Chem. Phys.* **2014**, *16*, 18545-18552.

(9) Mariano, R. G.; McKelvey, K.; White, H. S.; Kanan, M. W. *Science* **2017**, *358*, 1187-1192.

(10) Momotenko, D.; Byers, J. C.; McKelvey, K.; Kang, M.; Unwin, P. R. *ACS Nano* **2015**, *9*, 8942-8952.

(11) Bentley, C. L.; Kang, M.; Unwin, P. R. *J Am Chem Soc* **2017**, *139*, 16813-16821.

(12) Bentley, C. L.; Unwin, P. R. *Faraday Discuss.* **2018**, *210*, 365-379.

(13) Bentley, C. L.; Kang, M.; Maddar, F. M.; Li, F.; Walker, M.; Zhang, J.; Unwin, P. R. *Chem. Sci.* **2017**, *8*, 6583-6593.

(14) Bentley, C. L.; Andronescu, C.; Smialkowski, M.; Kang, M.; Tarnev, T.; Marler, B.; Unwin, P. R.; Apfel, U. P.; Schuhmann, W. *Angewandte Chemie International Edition* **2018**, *57*, 4093-4097.

(15) Inomata, H.; Takahashi, Y.; Takamatsu, D.; Kumatani, A.; Ida, H.; Shiku, H.; Matsue, T. *Chemical Communications* **2019**, *55*, 545-548.

(16) Yule, L. C.; Bentley, C. L.; West, G.; Shollock, B. A.; Unwin, P. R. *Electrochimica Acta* **2019**, *298*, 80-88.

(17) Ebejer, N.; Güell, A. G.; Lai, S. C. S.; McKelvey, K.; Snowden, M. E.; Unwin, P. R. *Annual Review of Analytical Chemistry* **2013**, *6*, 329-351.

(18) Bentley, C. L.; Kang, M.; Unwin, P. R. *Current Opinion in Electrochemistry* **2017**, *6*, 23-30.

(19) Chen, C.-H.; Jacobse, L.; McKelvey, K.; Lai, S. C. S.; Koper, M. T. M.; Unwin, P. R. *Analytical Chemistry* **2015**, *87*, 5782-5789.

(20) E, S. P.; Kim, Y.-R.; Perry, D.; Bentley, C. L.; Unwin, P. R. *ACS Applied Materials & Interfaces* **2016**, *8*, 30458-30466.

(21) Takahashi, Y.; Kumatani, A.; Munakata, H.; Inomata, H.; Ito, K.; Ino, K.; Shiku, H.; Unwin, P. R.; Korchev, Y. E.; Kanamura, K.; Matsue, T. *Nature Communications* **2014**, *5*, 5450.

(22) Ali, G. A. M.; Yusoff, M. M.; Ng, Y. H.; Lim, H. N.; Chong, K. F. *Current Applied Physics* **2015**, *15*, 1143-1147.

(23) Talaie, E.; Bonnick, P.; Sun, X.; Pang, Q.; Liang, X.; Nazar, L. F. *Chemistry of Materials* **2017**, *29*, 90-105.

(24) Martínez-Paredes, G.; González-García, M. B.; Costa-García, A. *Electrochimica Acta* **2009**, *54*, 4801-4808.

(25) Benck, J. D.; Hellstern, T. R.; Kibsgaard, J.; Chakthranont, P.; Jaramillo, T. F. *ACS Catalysis* **2014**, *4*, 3957-3971.

(26) Anantharaj, S.; Ede, S. R.; Karthick, K.; Sam Sankar, S.; Sangeetha, K.; Karthik, P. E.; Kundu, S. *Energy Environ. Sci.* **2018**, *11*, 744-771.

(27) Tao, B.; Yule, L. C.; Daviddi, E.; Bentley, C. L.; Unwin, P. R. *Angewandte Chemie International Edition* **2019**, *10.1002/anie.201814505*.

(28) Snowden, M. E.; Dayeh, M.; Payne, N. A.; Gervais, S.; Mauzeroll, J.; Schougaard, S. B. *Journal of Power Sources* **2016**, *325*, 682-689.

(29) Harris, P. J. F. *Philosophical Magazine* **2004**, *84*, 3159-3167.

(30) Patel, A. N.; Collignon, M. G.; O'Connell, M. A.; Hung, W. O. Y.; McKelvey, K.; Macpherson, J. V.; Unwin, P. R. *Journal of the American Chemical Society* **2012**, *134*, 20117-20130.

(31) Novoselov, K. S.; Geim, A. K.; Morozov, S. V.; Jiang, D.; Zhang, Y.; Dubonos, S. V.; Grigorieva, I. V.; Firsov, A. A. *Science* **2004**, *306*, 666-669.

(32) Spitzer, P.; Wunderli, S.; Maksymiuk, K.; Michalska, A.; Kisiel, A.; Galus, Z.; Tauber, G. In *Handbook of Reference Electrodes*, Inzelt, G.; Lewenstam, A.; Scholz, F., Eds.; Springer Berlin Heidelberg: Berlin, Heidelberg, 2013, pp 77-143.

(33) Bentley, C. L.; Kang, M.; Maddar, F.; Li, F.; Walker, M.; Zhang, J.; Unwin, P. R. *Chemical Science* **2017**.

(34) Snowden, M. E.; Güell, A. G.; Lai, S. C. S.; McKelvey, K.; Ebejer, N.; O'Connell, M. A.; Colburn, A. W.; Unwin, P. R. *Analytical Chemistry* **2012**, *84*, 2483-2491.

(35) Bentley, C. L.; Perry, D.; Unwin, P. R. *Anal. Chem.* **2018**, *90*, 7700-7707.

(36) McKelvey, K.; Kinnear, S. L.; Perry, D.; Momotenko, D.; Unwin, P. R. *J Am Chem Soc* **2014**, *136*, 13735-13744.

(37) Bard, A. J.; Faulkner, L. R. *Electrochemical Methods: Fundamentals and Applications*; John Wiley and Sons Inc., 2001.

(38) Schmickler, W.; Santos, E. *Interfacial Electrochemistrty*, 2 ed.; Springer, Berlin, Heidelberg, 2010, p 272.

(39) Sand, H. J. S. *The London, Edinburgh, and Dublin Philosophical Magazine and Journal of Science* **1901**, *1*, 45-79.

(40) Saito, Y. *Review of Polarography* **1968**, *15*, 177-187.

(41) Aoki, K.; Akimoto, K.; Tokuda, K.; Matsuda, H.; Osteryoung, J. *Journal of Electroanalytical Chemistry and Interfacial Electrochemistry* **1985**, *182*, 281-294.

(42) Fleischmann, M.; Pons, S. *Journal of Electroanalytical Chemistry and Interfacial Electrochemistry* **1988**, *250*, 257-267.

(43) Abrantes, L. M.; Fleischmann, M.; Li, L. J.; Hawkins, M.; Pons, J. W.; Daschbach, J.; Pons, S. *Journal of Electroanalytical Chemistry and Interfacial Electrochemistry* **1989**, *262*, 55-66.

(44) Hinnemann, B.; Moses, P. G.; Bonde, J.; Jørgensen, K. P.; Nielsen, J. H.; Horch, S.; Chorkendorff, I.; Nørskov, J. K. *Journal of the American Chemical Society* **2005**, *127*, 5308-5309.

(45) Jaramillo, T. F.; Jørgensen, K. P.; Bonde, J.; Nielsen, J. H.; Horch, S.; Chorkendorff, I. *Science* **2007**, *317*, 100-102.

(46) Seh, Z. W.; Kibsgaard, J.; Dickens, C. F.; Chorkendorff, I.; Nørskov, J. K.; Jaramillo, T. F. *Science* **2017**, *355*, 146.

(47) Ooka, H.; Figueiredo, M. C.; Koper, M. T. M. *Langmuir* **2017**, *33*, 9307-9313.

(48) Cave, E. R.; Shi, C.; Kuhl, K. P.; Hatsukade, T.; Abram, D. N.; Hahn, C.; Chan, K.; Jaramillo, T. F. *ACS Catalysis* **2018**, 3035-3040.

(49) Esmaily, M.; Svensson, J. E.; Fajardo, S.; Birbilis, N.; Frankel, G. S.; Virtanen, S.; Arrabal, R.; Thomas, S.; Johansson, L. G. *Progress in Materials Science* **2017**, *89*, 92-193.